

Article

State-of-Health Prediction of Lithium-Ion Batteries Based on CNN-BiLSTM-AM

Yukai Tian ¹, Jie Wen ^{1,*}, Yanru Yang ¹, Yuanhao Shi ¹ and Jianchao Zeng ²¹ School of Electrical and Control Engineering, North University of China, Taiyuan 030051, China² School of Data Science and Technology, North University of China, Taiyuan 030051, China

* Correspondence: wenjie@nuc.edu.cn

Abstract: State-of-Health (SOH) prediction of lithium-ion batteries is crucial in battery management systems. In order to guarantee the safe operation of lithium-ion batteries, a hybrid model based on convolutional neural network (CNN)-bidirectional long short-term memory (BiLSTM) and attention mechanism (AM) is developed to predict the SOH of lithium-ion batteries. By analyzing the charging and discharging process of batteries, the indirect health indicator (HI), which is highly correlated with capacity, is extracted in this paper. HI is taken as the input of CNN, and the convolution and pooling operations of CNN layers are used to extract the features of battery time series data. On this basis, a BiLSTM depth model is built in this paper to collect the data coming from CNN forward and reverse dependencies and further emphasize the correlation between the serial data by AM to obtain an accurate SOH estimate. Experimental results based on NASA PCoE lithium-ion battery data demonstrate that the proposed hybrid model outperforms other single models, with the root mean square error (RMSE) of SOH prediction results all less than 0.01, and can accurately predict the SOH of lithium-ion batteries.



Citation: Tian, Y.; Wen, J.; Yang, Y.; Shi, Y.; Zeng, J. State-of-Health Prediction of Lithium-Ion Batteries Based on CNN-BiLSTM-AM. *Batteries* **2022**, *8*, 155. <https://doi.org/10.3390/batteries8100155>

Academic Editor: Joeri Van Mierlo

Received: 15 August 2022

Accepted: 29 September 2022

Published: 3 October 2022

Publisher's Note: MDPI stays neutral with regard to jurisdictional claims in published maps and institutional affiliations.



Copyright: © 2022 by the authors. Licensee MDPI, Basel, Switzerland. This article is an open access article distributed under the terms and conditions of the Creative Commons Attribution (CC BY) license (<https://creativecommons.org/licenses/by/4.0/>).

1. Introduction

The lithium-ion battery industry is an essential precursor to the world's advanced technology development [1]. With the characteristics of higher energy density, higher power density, higher conversion rate, longer cycle time, and less pollution, lithium-ion batteries are extensively applied in electric vehicles and various energy storage systems [2]. Lithium-ion batteries are now being applied more widely in mobile communications, transportation, electrical energy storage, new energy resources in storage, and aerospace [3]. Considering the widespread application of lithium-ion batteries, the secure operation of lithium-ion batteries must be given paramount importance, and the state of health (SOH) is the most critical parameter for evaluating the current state and performance of lithium-ion batteries [4]. Consequently, optimizing the design and management of lithium-ion batteries and accurately predicting the SOH of lithium-ion batteries is essential to assessing degradation and aging mechanisms.

The methods for predicting lithium-ion batteries can be classified into three groups: model-based methods [5–10], data-driven methods [11–13], and hybrid methods [14,15]. Model-based methods require extensive knowledge in the field of physical chemistry, understanding the reaction mechanisms internal to the battery, accurately describing the mathematical equations for the internal reactions, and building efficient simulation models, which can be difficult in practical applications. Data-driven approaches have been demonstrated to be one of the most significant methods for modelling battery degradation and assessing battery SOH due to their flexibility and the lack of need to build models of physical mechanisms such as artificial neural networks [16–18], relevance vector machine [19,20],

Gaussian process regression [21,22], etc. Deep learning has been gaining more and more attention when it comes to SOH prediction for lithium-ion batteries [23–25]. For instance, Chaoui et al. proposed a simple Recurrent Neural Network (RNN)-based approach to estimate the SOH of lithium-ion batteries using a dynamically driven RNN [26]. Chen et al. used constant current discharge time, the charge/discharge cycle number, and charge capacity to build a long- and short-term memory network (LSTM) model to enable SOH prediction for lithium-ion batteries [27]. Hybrid methods are combinations of two or several models that use the same or different types of methods for SOH prediction. Bezha et al. combined Convolutional Neural Network (CNN) and LSTM for battery SOH prediction, taking the current–voltage profile as input and SOH as output, and it is demonstrated that the proposed hybrid method has the advantage of providing accurate estimates in terms of SOH [28]. Qu et al. developed an LSTM model and combined LSTM with particle swarm optimization (PSO) and Attention Mechanism (AM) to achieve monitoring and prediction of SOH for lithium-ion batteries. The results demonstrate a high level of accuracy of the estimates [29].

In summary, the single data-driven model cannot take into account feature extraction from lithium-ion batteries and accurate SOH prediction. Therefore, highly accurate models and methods are needed to achieve the SOH prediction of lithium-ion batteries. It is considered that the correlation between input data can be enhanced by AM and has an application to many forecasting tasks, for instance, stock forecasting and electricity forecasting [30–34]. The CNN-BiLSTM-AM model is presented in this paper to predict the SOH of lithium-ion batteries, and integrates the merits of CNN and BiLSTM. In the proposed CNN-BiLSTM-AM model, the convolution and pooling operations of the CNN layer are utilized to extract the features of the battery time series data, while the BiLSTM depth model is used to collect the forward and reverse dependencies of the CNN incoming data, which further emphasizes the correlation of the time series data and capturing long-term dependencies. In addition, the time series data associated with SOH are weighted by AM resulting in an accurate SOH prediction for lithium-ion batteries.

The remainder of this paper is organized as follows. The used basic theoretical knowledge is described in Section 2. Dataset description and data preprocessing for lithium-ion batteries SOH prediction are presented in Section 3. In Section 4, the proposed CNN-BiLSTM-AM model is described, while Section 5 presents the experimental settings. Based on a NASA dataset, the CNN-BiLSTM-AM model is used to predict the SOH of lithium-ion batteries in Section 6. Lastly, we summarize and discuss briefly possible future directions for this paper in Section 7.

2. Preliminaries

This section will briefly introduce the basic theoretical knowledge of CNN, BiLSTM, and AM used in the CNN-BiLSTM-AM model presented in this paper.

2.1. CNN

CNN has an exceptional ability to capture features of spatial data, and it has played an instrumental role in the recent development of deep learning. It comprises three main types of layers: the convolutional layer, the pooling layer, and the fully connected layer. Its output is as follows:

$$y_t = \tanh(W_t X_t + b_t) \quad (1)$$

where X_t and y_t are the input and output, respectively; \tanh is the activation function; W_t and b_t represent the weight and bias, respectively.

A prototypical CNN unit is shown in Figure 1. The convolutional layer extracts local features by the size of the filter, and the features extracted by the pooling layer selection, which reduces the sophistication of the network parameters and structure, while the fully connected layer is a neural layer with an activation function that maps the relationship between input and output in a non-linear way. Since the convolution operations use the same set of weights, this reduces the number of parameters in CNN and solves the

problem of overfitting. As a consequence, CNN is extensively used to predict the time series. Nevertheless, the increased sensitivity to sparse data is a drawback of CNN, and CNN is likely to be restricted to cases where good data are easily available. Thus, this paper collects the forward and backward dependencies of the data coming from CNN by building a BiLSTM depth model.

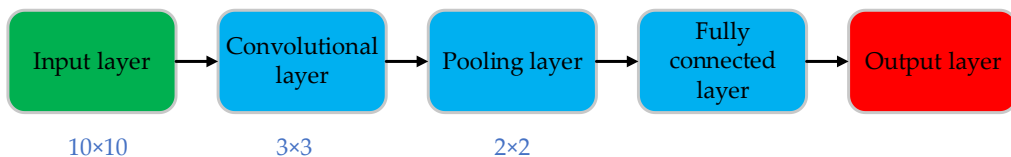


Figure 1. Prototypical CNN unit.

2.2. BiLSTM

Since lithium-ion battery data are collected during the charging and discharging cycles, they belong to the time series. RNN is applicable to processing time series, which help RNN process information in an orderly manner. To address the problem of exploding or disappearing gradients in RNN, the network structure of LSTM is proposed, substituting the state unit of classical RNN with the recurrent unit structure of LSTM.

A particular type of RNN model is LSTM. Compared to RNN, LSTM can better handle long-term continuous data. LSTM has three gate controls, i.e., the forget gate, the input gate, and the output gate, respectively. Figure 2 shows a prototype LSTM unit.

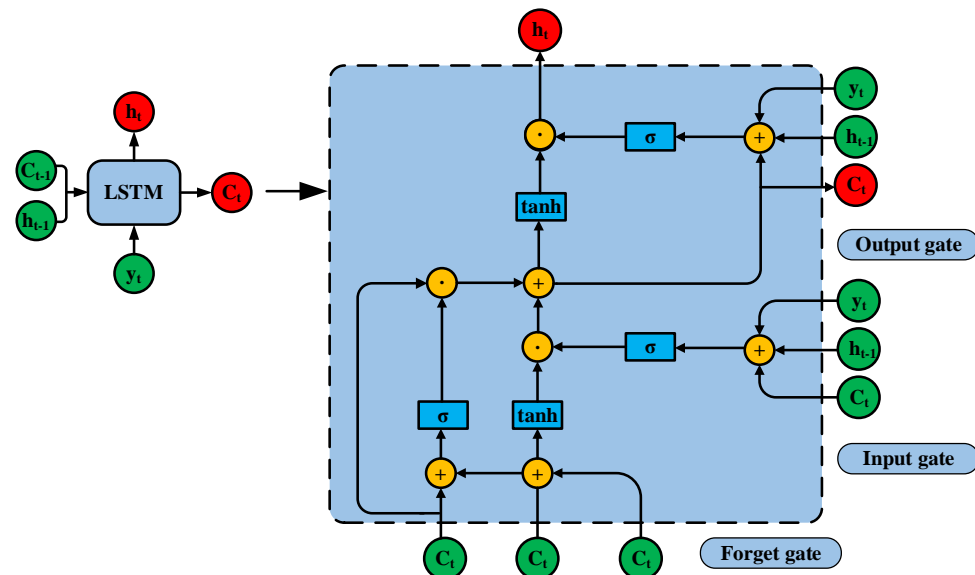


Figure 2. Recurrent unit structure of LSTM network.

The main role of the forgetting gate is to store information about when unit values ought to be forgotten, given by the following equation:

$$f_t = \sigma(W_f \cdot [y_t, h_{t-1}] + b_f) \quad (2)$$

where y_t represents the input value; h_{t-1} represents the output value; W_f, b_f represents the weight and bias, respectively, and σ is the activation function.

The input gate stores the values into a memory unit, which operates as follows:

$$i_t = \sigma(W_i \cdot [y_t, h_{t-1}] + b_i) \quad (3)$$

$$\tilde{C}_t = \tanh(W_c \cdot [y_t, h_{t-1}] + b_c) \quad (4)$$

where W_i, W_c are weights; \tanh is the activation function, and \tilde{C}_t is a one-dimensional matrix with values ranging from 0 to 1.

Combining the output of the forget and input gates, the information as C_t is updated by:

$$C_t = f_t \cdot C_{t-1} + i_t \cdot \tilde{C}_t \quad (5)$$

The output gate controls the reading of the value of the memory unit.

$$o_t = \sigma(W_o \cdot [y_t, h_{t-1}] + b_o) \quad (6)$$

where W_o, b_o are the weight and bias of the output gate, respectively, and o_t is the output of the LSTM. The hidden state at time step t is updated in the following manner:

$$h_t = o_t \cdot \tanh(C_t) \quad (7)$$

A BiLSTM consisting of a two-layer LSTM is shown in Figure 3, where the predicted system state is referred to a sequence of outputs from the bidirectional incoming LSTM layer. The predicted results are merged and assigned to the next LSTM layer; after the second LSTM layer, the ultimate prediction is determined by forward and backward propagation together. The BiLSTM depth model can better collect the bidirectional dependency of data from CNN than the LSTM model. Therefore, the model proposed in this paper is chosen as BiLSTM to enhance the accuracy of SOH prediction for lithium-ion batteries.

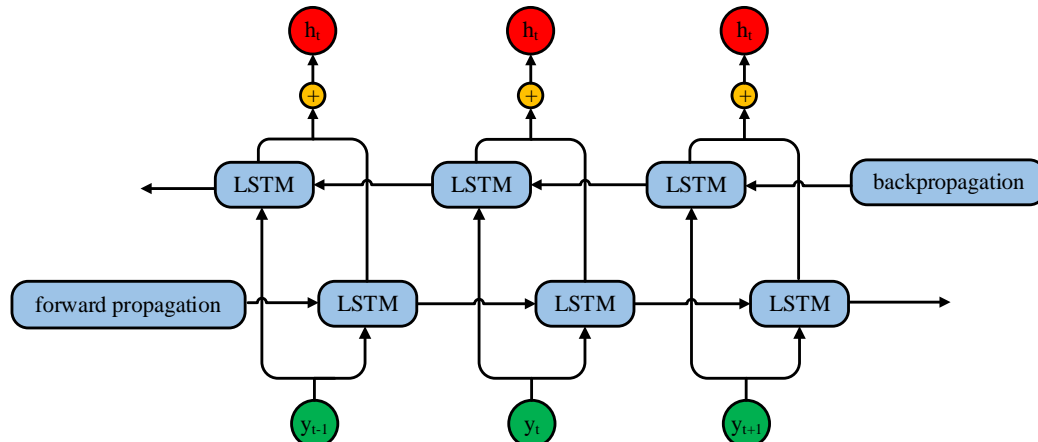


Figure 3. Recurrent unit structure of BiLSTM networks.

2.3. AM

Recently, scholars have applied AM to neural networks based on the concerns of the human brain AM and achieved excellent prediction results. In neural networks, each feature has a different impact on the outcome, but usually only a group of features determines the output. The main mechanism of AM is to follow the learning based on the attention level of the individual features in the series, and to integrate the features according to this attention level. To tackle the problem of attention distraction, this paper introduces AM, which sets weights for each feature according to its impact on the result. Figure 4 is a schematic diagram of the structure of the AM.

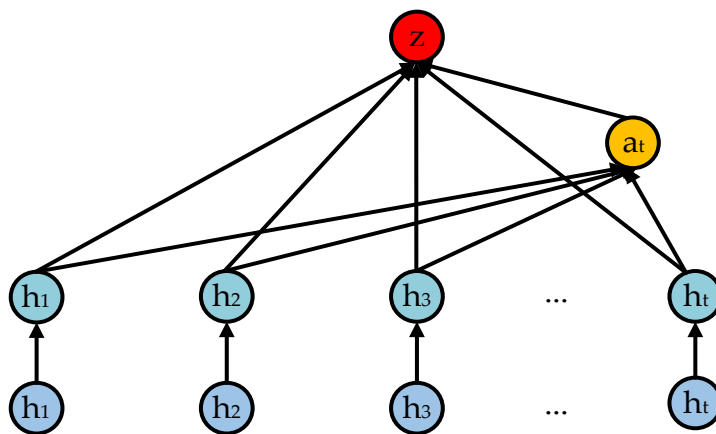


Figure 4. Structure diagram of AM.

The expressions for the calculation of AM are shown in (8)–(10).

$$u_t = \tanh(W_w h_t + b_w) \quad (8)$$

$$a_t = \text{softmax}(u_t^T, u_w) \quad (9)$$

$$z = \sum a_t h_t \quad (10)$$

where W_w is first randomly initialized and then determined through the network training process; u_w is weight; b_w represents bias; a_t represents the weight of each attribute; z represents the prediction result after weighted summation.

3. Dataset Description and Data Preprocessing

3.1. Dataset Description

To train and test the proposed model, B0005, B0006, and B0018 of the NASA PCoE battery dataset are selected in this paper [35]. Charge, discharge, and impedance operation of three lithium-ion batteries is carried out at room temperature (24 °C). To start with, there is a charging process in which each battery at a constant current of 1.5 A until it reaches a voltage of 4.2 V. This is followed by charging in a constant voltage mode until the charging current drops to 20 mA. Secondly, there is a discharging process in which each battery is discharged under a constant current of 2 A until each battery's voltage drops to 2.7 V, 2.5 V, and 2.5 V, respectively. Finally, there is an impedance process using electrochemical impedance spectra swept from 0.1 Hz to 5 kHz. The information of batteries B0005, B0006, and B0018 are displayed in Table 1.

Table 1. NASA dataset lithium-ion battery information.

Battery	Number of Charges	Number of Discharges	Number of Impedances	Actual Life Expectancy
B0005	170	168	278	124
B0006	170	168	278	108
B0018	134	132	53	96

As can be observed in Figure 5, the three batteries gradually decrease in capacity through time and are accompanied by rebound in capacity during the degradation process. All three batteries are subjected to charge and discharge cycles, and once the batteries have dropped 30% of their nominal capacity, the end-of-life (EOL) point is reached, that is, from 2 Ah to 1.4 Ah.

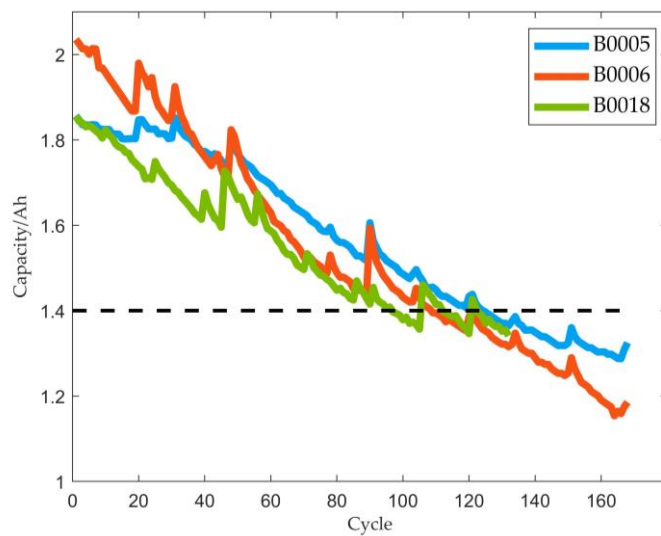


Figure 5. Capacity degradation curve of lithium-ion batteries.

3.2. Data Preprocessing

The most intuitive manifestation of battery degradation is the decay in capacity, which is predominantly related to the SOH of the battery. SOH is defined by capacity and given by the following equation [36]:

$$SOH = \frac{C_{actual}}{C_{nom}} \times 100\% \quad (11)$$

where C_{actual} and C_{nom} represent the actual and nominal capacities, respectively.

Lithium-ion battery time series data for predicting SOH and the data preprocessing include data cleaning and normalization.

For better prediction accuracy and performance of deep learning models, experimental data need to be handled. To begin with, the data are cleaned by removing outliers and missing values, which are evaluated by moving averages or intermediate values, which cause the battery data to demonstrate periodic degradation characteristics. The battery specifications and data collection conditions have been summarized in Table 1. Data preprocessing assures that there are no erroneous values that could confound the model, as well as also being periodically averaged to avoid short-term fluctuations.

Data normalization is commonly applied in depth modelling algorithms where it is appropriate to improve the convergence of the model and the accuracy of the prediction. Normalization will be performed by the minimum–maximum method, where the data are scaled between 0 and 1. This is described by the following equation.

$$x_n = \frac{x - x_{min}}{x_{max} - x_{min}} \quad (12)$$

where x_n represents the processed data; x represents the original data; x_{max}, x_{min} represent the maximum and minimum values of the original data, respectively.

4. Methods

4.1. CNN-BiLSTM-AM Model

In this paper, the CNN-BiLSTM-AM model is proposed, which combines the characteristics and merits of CNN, BiLSTM, and AM to predict the SOH of lithium-ion batteries.

The model structure of CNN-BiLSTM-AM is presented in Figure 6, which primarily composed of the input layer, CNN layer, BiLSTM layer, AM layer, and output layer.

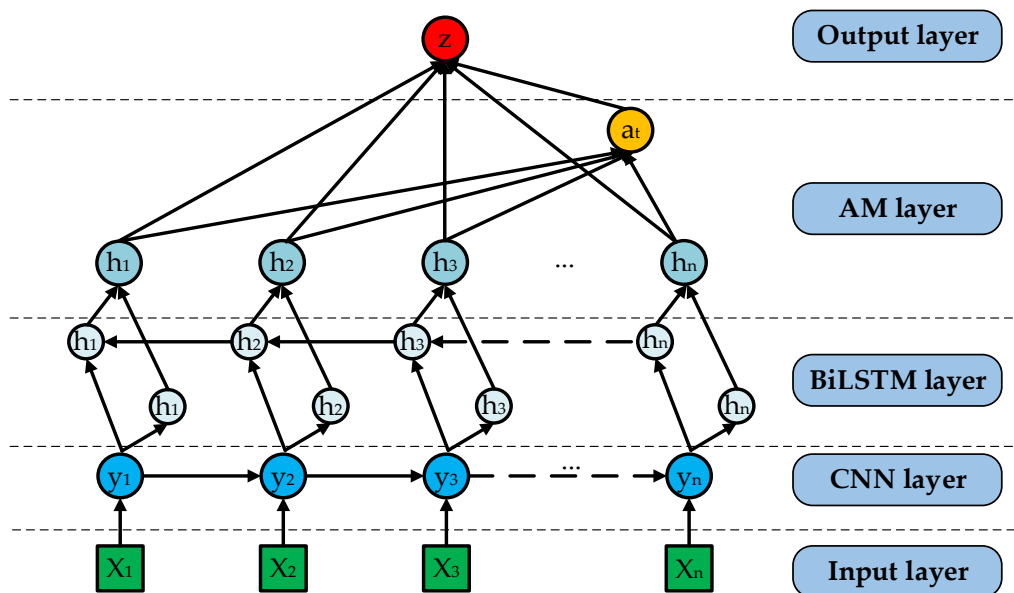


Figure 6. Structure diagram of CNN-BiLSTM-AM.

The model structure of CNN-BiLSTM-AM is described in detail as follows.

- (1) Input layer: Firstly, HIs that can characterize the capacity during the charging and discharging process of the lithium-ion battery dataset are extracted, and those that are highly correlated with the capacity are selected as indirect HI; the indirect HI is preprocessed with the data, the processed dataset is divided, and the HI of the training set is used as the input of CNN.
- (2) CNN layer: Including innovative concepts such as shared weight and local perceptual fields means CNN has unique benefits in processing battery datasets. In this paper, we use the convolution and pooling operations from the battery time series data to extract features.
- (3) BiLSTM layer: The BiLSTM depth model is built, which is made up of forwarding and inverse LSTM. In comparison with the LSTM, the BiLSTM can extract time series in both directions and better collect the forward and reverse dependencies of the data coming from the CNN.
- (4) AM layer: AM has been introduced into the hybrid model with the objective of enhancing the accuracy of the prediction model. AM assigns that each feature has a weight, further emphasizing the correlation between the data, which raises the accuracy of the prediction model.
- (5) Output layer: The weighted summed prediction results from the AM layer are output and then the testing set is fed into the trained model for prediction to generate SOH prediction results.

4.2. Prediction Procedure Based on CNN-BiLSTM-AM Model

Flow chart of SOH prediction based on CNN-BiLSTM-AM model is in Figure 7, from which one can see that the prediction procedure of SOH is comprised of the following five steps.

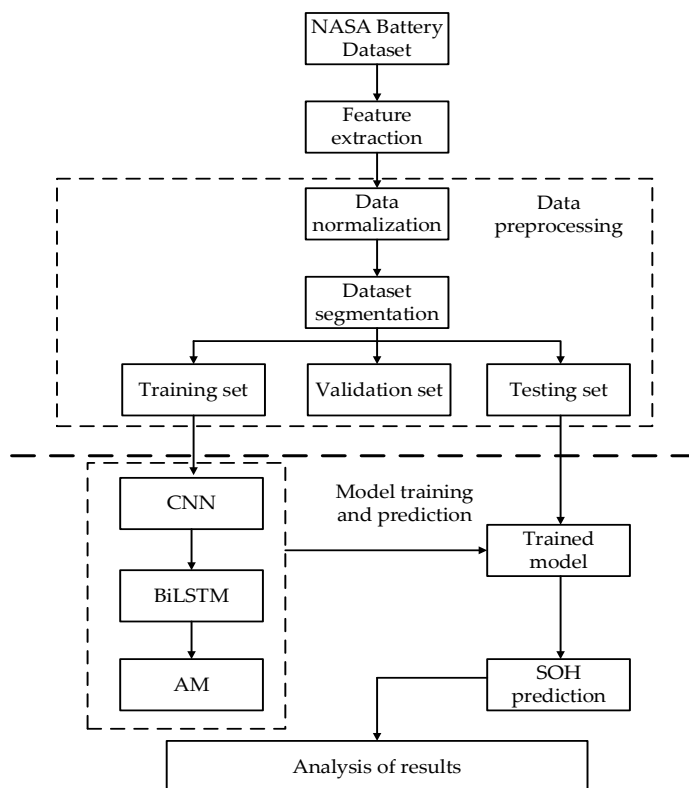


Figure 7. Flow chart of SOH prediction based on CNN-BiLSTM-AM model.

- Step 1. Feature Extraction: Initially, indirect HIs that reflect battery capacity degeneration are extracted by considering the charge and discharge voltage, current, and temperature curves of lithium-ion batteries, and those that are highly correlated with capacity are selected as indirect HIs.
- Step 2. Data Preprocessing: The extracted HI is normalized as well as followed by segmentation of the dataset.
- Step 3. Build the model and Train: The convolution and pooling operations of the CNN layer are used to extract features, and the bidirectional dependencies of the data coming from CNN are collected by the BiLSTM depth model, followed by the time series data related to SOH weighted by AM, so as to build the CNN-BiLSTM-AM model, and the hyperparameters of the model are determined using the grid search method during the model training process to derive the optimal model.
- Step 4. Model Prediction: The testing set is fed into the trained model for prediction, resulting in SOH prediction results.
- Step 5. Analysis of Results: Lastly, to further verify the validity of the proposed model, three comparison models of CNN, BiLSTM, and CNN-BiLSTM are designed, and the SOH prediction model is quantitatively evaluated using error evaluation metrics.

5. Experimental Settings

5.1. Experimental Equipment and Model Parameter Settings

The experimental environment utilized in this paper has been described as follows. Hardware environment: Intel (R) Core (TM) i5-6300HQ CPU @ 2.30 GHz 2.30 GHz, 8 GB RAM, 64-bit operating system. The model is implemented in Python 3.7 using Keras.

In this paper, three datasets are used for the SOH prediction of lithium-ion batteries. The datasets are divided into training set, validation set, and testing set. The training set serves to train the model, validation set to adjust the parameters, and testing set for assessing the performance of the model. The details of the division are presented in Table 2.

Table 2. Dataset segmentation.

Dataset	Training Set	Validation Set	Testing Set
B0005	(70%) 50	37	(30%) 37
	(80%) 74	25	(20%) 25
	(90%) 99	12	(10%) 13
B0006	(70%) 43	32	(30%) 33
	(80%) 65	22	(20%) 21
	(90%) 86	11	(10%) 11
B0018	(70%) 38	29	(30%) 29
	(80%) 58	19	(20%) 19
	(90%) 77	10	(10%) 9

A number of appropriate hyperparameters need to be selected in the model to guarantee the accuracy of the model predictions. Model performance is frequently validated using grid search and cross-validation to obtain optimum parameters. The K values for cross-validation may impact how sensitive they are to changes in the training set, hence affecting the hyperparameter results. The grid search method will be applied to determine the hyperparameters. The parameters are set as in Table 3.

Table 3. Parameter setting.

Parameter	Setting Value
Optimizer	Adam
Loss function	MSE
Activation function	RELU
Filter size	10
Batch size	16
Epochs	1000
Dropout rate	0.200
Learning rate	0.001
Number of neurons	160

In CNN convolutional model, too few convolutional and pooling layers will contribute to the inadequate extraction of critical local information, while too many will result in a longer run time and extraction of too much invalid information. When the batch size is too large, the optimization of the loss function and gradient descent is detrimental and can cause large errors. If the batch size is too small, the time consumption of the neural network may be greatly extended, and eventually, the dropout layer is inserted to prevent overfitting and boost the training speed.

5.2. Performance Evaluation Indicators

Three error evaluation metrics are used in this paper, i.e., Root Mean Square Error (RMSE), Mean Absolute Error (MAE), and Mean Absolute Percentage Error (MAPE), which are presented to provide a quantitative assessment of the accuracy of the proposed SOH prediction model and defined as:

$$RMSE = \sqrt{\frac{1}{N} \sum_{i=1}^N (y_i - \hat{y}_i)^2} \quad (13)$$

$$MAE = \frac{1}{N} \sum_{i=1}^N |y_i - \hat{y}_i| \quad (14)$$

$$MAPE = \frac{1}{N} \sum_{i=1}^N \left| \frac{y_i - \hat{y}_i}{y_i} \right| \times 100\% \quad (15)$$

where y_i is the real SOH value and \hat{y}_i denotes the SOH predicted value. Specifically, for indicators such as RMSE, MAE, and MAPE, the closer they approached zero, the more accurate the prediction.

6. Experiment and Result Analysis of SOH Prediction

6.1. HI Extraction

We have successfully extracted the capacity degradation data of a group of three lithium-ion batteries of the same type from the NASA PCoE public dataset. By analyzing charge and discharge characteristics of the B0005 battery in the NASA dataset, as an illustration, it is demonstrated in Figure 8.

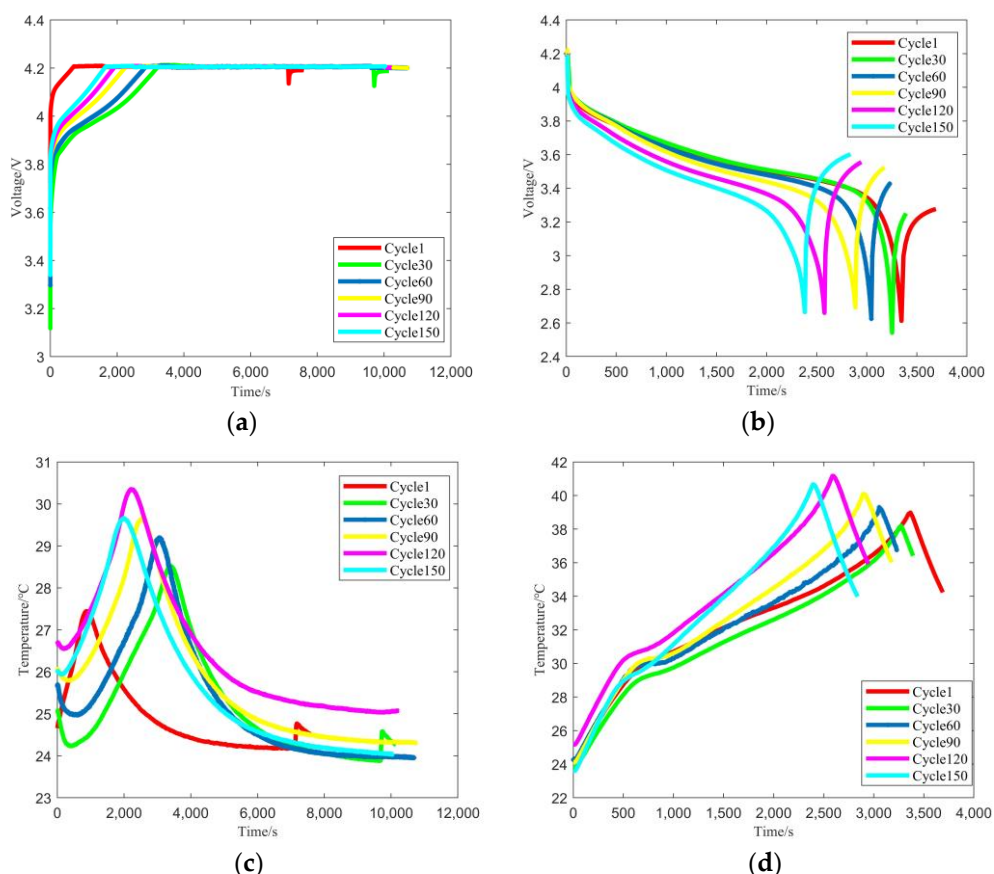


Figure 8. B0005 charge and discharge curves at different cycles. (a) Charge voltage curve; (b) Discharge voltage curve; (c) Charge temperature curve; (d) Discharge temperature curve.

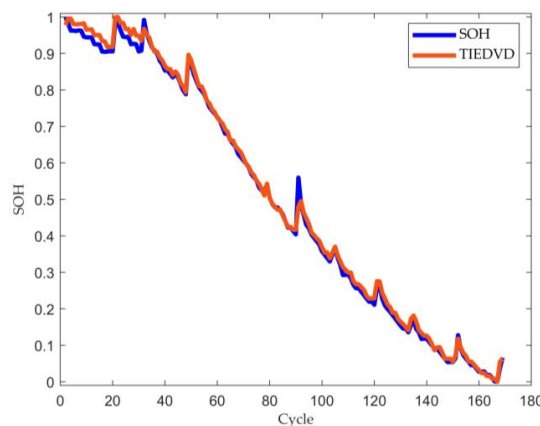
In Figure 8a, the charging process is constant voltage charging, so we have analyzed the discharging process. From Figure 8b, the voltage variation of the B0005 battery at different cycles in the discharging process, it is clear that there is rich degradation information in the voltage between 3.4 V and 3.8 V. In order to avoid information redundancy, the Time Interval of an Equal Discharging Voltage Difference (TIEDVD) is chosen as the time difference corresponding to 3.4–3.8 V, and the 150th cycle is taken as an illustration.

On this basis, we have extracted four HIs: the time at which the discharge voltage reaches its minimum point, the maximum gradient of the voltage curve in the initial stage of the discharge process, the discharge power, and the time it takes for the temperature to reach the peak value during the discharge process. Table 4 presents the results of the Pearson correlation analysis of HI and capacity of B0005, from which it can be noticed that TIEDVD has the highest correlation with the capacity of lithium-ion battery.

Table 4. Correlation analysis of HI and capacity of B0005.

HI	Pearson
TIEDVD	0.9972
Time at which the discharge voltage reaches its minimum point	0.9928
Maximum gradient of the voltage curve in the initial stage of the discharge process	0.8050
Discharge power	0.9132
Time it takes for the temperature to reach the peak value during the discharge process	0.9886

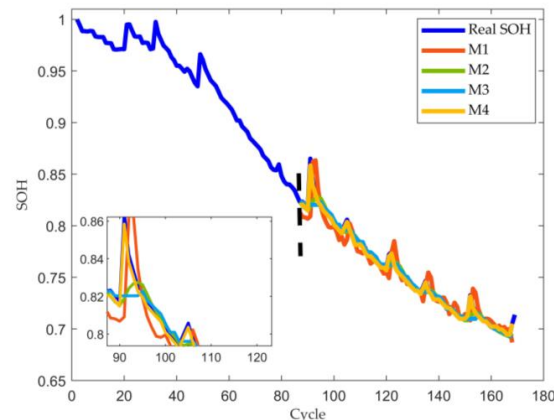
Figure 9 presents a qualitative analysis of SOH and TIEDVD, from which one can see that TIEDVD follows the same trend as that of SOH, and the rebound part can be followed better. As a result, TIEDVD works as HI to predict the SOH of lithium-ion batteries.

**Figure 9.** Qualitative analysis of SOH and TIEDVD.

6.2. Results and Analysis of SOH Prediction

To demonstrate the effectiveness of the proposed CNN-BiLSTM-AM model, three models, i.e., CNN model, BiLSTM model, CNN-BiLSTM model, are designed to make a comparison with the CNN-BiLSTM-AM model for different prediction Starting Points (SPs) in this subsection, and the CNN model, BiLSTM model, CNN-BiLSTM model, and CNN-BiLSTM-AM model are represented as M1, M2, M3, and M4, respectively.

Firstly, the B0005 battery is selected for prediction at SP = 70%, and the prediction results of the B0005 battery are presented in Figure 10. It is evident from Figure 10 that the M1 model for the B0005 battery shows the largest error, of which the M2 and M3 models are the next largest. With the best prediction performance of the M4 model for trend degradation and capacity rebound, and the predicted values being closest to the real SOH value, the validity of the CNN-BiLSTM-AM model introduced in this paper is verified.

**Figure 10.** Different models of SOH prediction results for B0005.

A setup of SOH predictions for the same battery at different SPs has been carried out to demonstrate further the accuracy of the presented model (M4). The prediction results of SOH for the B0005 battery at different SPs are shown in Figure 11. The BiLSTM model in the M4 model collects the bidirectional dependence of the incoming CNN data, AM further emphasizes the correlation between the serial data by weighting, and the SP = 90% follows the same pattern of variation. In addition, the prediction results of M4 are similar to the real SOH values at different SPs, and more accurate predictions are obtained, especially for the capacity reversion. Furthermore, Figure 11 presents that the error of the prediction results for SP = 70%, SP = 80%, and SP = 90% are smaller, which further proves the high accuracy of the CNN-BiLSTM-AM model.

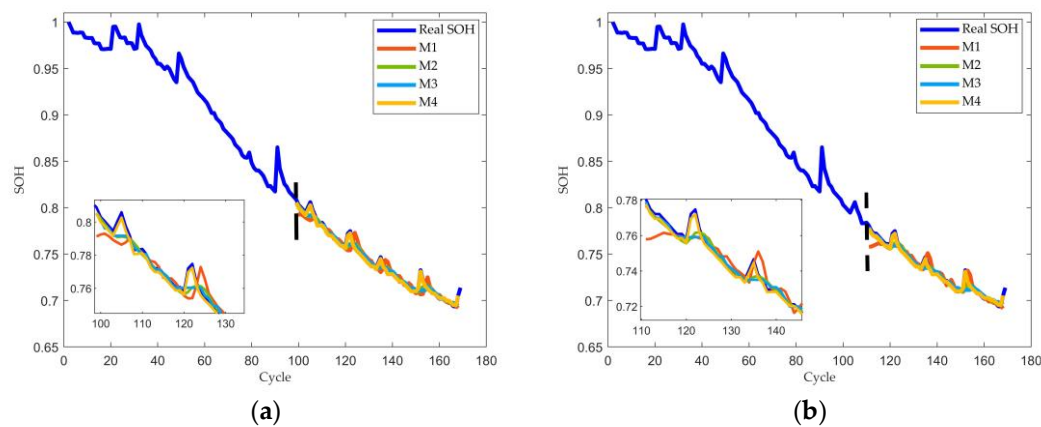


Figure 11. SOH prediction results for B0005 at different SPs. (a) SP = 80%; (b) SP = 90%.

RMSE, MAE, and MAPE have been adopted as error evaluation metrics to quantitatively assess the accuracy of the CNN-BiLSTM-AM prediction model. Table 5 illustrates the prediction results of SOH based on different models for batteries B0005, B0006, and B0018 with different SPs. In Table 5, the smallest RMSE, MAE, and MAPE are 0.00487, 0.00307, and 0.420%, respectively, corresponding to the M4 model for the B0005 battery at SP = 90%; the largest RMSE, MAE, and MAPE are 0.0153, 0.0121, and 1.60%, respectively, corresponding to the M1 model for the B0018 battery at SP = 90%. While the magnitude of the capacity rebound portion of the B0018 battery is larger, the M4 model is also accurately validated. The error of the M4 model for all three batteries are lower than the comparison models, with RMSE lower than 0.0120, MAE lower than 0.007, and MAPE lower than 0.9%. According to the results, the M4 model has the highest accuracy and the lowest prediction error.

Table 5. Prediction results of SOH based on different models for batteries B0005, B0006, and B0018 with different SPs.

Battery	Prediction SP	Model	RMSE	MAE	MAPE (%)
B0005	87 (70%)	M1	0.00893	0.00565	0.738
		M2	0.00867	0.00540	0.702
		M3	0.00794	0.00531	0.692
		M4	0.00737	0.00382	0.496
	99 (80%)	M1	0.00863	0.00661	0.886
		M2	0.00620	0.00432	0.582
		M3	0.00595	0.00432	0.581
		M4	0.00481	0.00316	0.425
B0018	111 (90%)	M1	0.00813	0.00633	0.825
		M2	0.00600	0.00409	0.558
		M3	0.00598	0.00408	0.558
		M4	0.00487	0.00307	0.420

Table 5. Cont.

Battery	Prediction SP	Model	RMSE	MAE	MAPE (%)
B0006	75 (70%)	M1	0.0151	0.0101	1.49
		M2	0.0133	0.00838	1.24
		M3	0.0133	0.00846	1.25
		M4	0.0114	0.00485	0.709
	87 (80%)	M1	0.0134	0.00864	1.28
		M2	0.0129	0.00812	1.21
		M3	0.0117	0.00779	1.15
		M4	0.0105	0.00491	0.727
	97 (90%)	M1	0.00914	0.00708	1.11
		M2	0.00845	0.00617	0.963
		M3	0.00759	0.00567	0.883
		M4	0.00572	0.00361	0.561
B0018	67 (70%)	M1	0.0145	0.0110	1.44
		M2	0.0139	0.00997	1.30
		M3	0.0138	0.0118	1.421
		M4	0.0108	0.00612	0.797
	77 (80%)	M1	0.0151	0.0119	1.56
		M2	0.0133	0.00981	1.29
		M3	0.0141	0.0109	1.44
		M4	0.0109	0.00623	0.619
	87 (90%)	M1	0.0153	0.0121	1.60
		M2	0.0141	0.0109	1.45
		M3	0.0150	0.0121	1.60
		M4	0.0112	0.00627	0.828

To investigate the effect of EOL on prediction error, we take B0005 as an example, where the EOLs are selected 70%, 75%, and 80% respectively, and the dataset has been repartitioned. The prediction results are presented in Figure 12 and Table 6, from which one can see that the largest RMSE, MAE, and MAPE are 0.00737, 0.00382, and 0.496%, respectively, corresponding to the M4 model for B0005 batteries with EOL = 70%; the smallest RMSE, MAE, and MAPE are 0.00621, 0.00432, and 0.343%, respectively, corresponding to the M4 model for EOL = 80%. Thus, the prediction error becomes higher when the EOL is set as the smaller percent of the health indicator, which is particularly evident in MAPE.

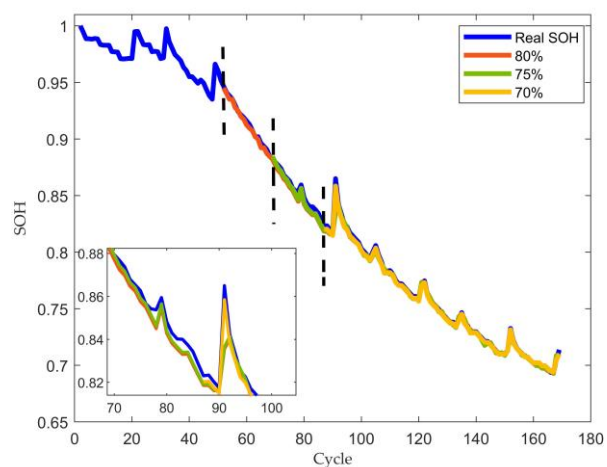
**Figure 12.** Different EOLs of SOH prediction results for B0005.

Table 6. Prediction results of SOH based on the M4 model for the B0005 battery with different EOLs.

EOL	Prediction SP	RMSE	MAE	MAPE (%)
70%	87 (70%)	0.00737	0.00382	0.496
	99 (80%)	0.00481	0.00316	0.425
	111 (90%)	0.00487	0.00307	0.420
75%	69 (70%)	0.00660	0.00465	0.364
	79 (80%)	0.00665	0.00454	0.355
	89 (90%)	0.00740	0.00383	0.499
80%	52 (70%)	0.00621	0.00432	0.343
	60 (80%)	0.00627	0.00435	0.343
	67 (90%)	0.00654	0.00457	0.357

7. Conclusions

Considering the security and dependability of lithium-ion batteries in real-world applications, a hybrid model based on CNN, BiLSTM, and AM is advanced to predict the SOH of lithium-ion batteries in this paper. In the CNN-BiLSTM-AM model, CNN is utilized to extract the features of the battery time series, BiLSTM to collect the bidirectional relationships, and AM to assign weights to achieve accurate SOH estimation of lithium-ion batteries. The prediction results of SOH by investigating different batteries with different SPs demonstrate that the proposed CNN-BiLSTM-AM model outperforms the CNN model, BiLSTM model, and CNN-BiLSTM model, with RMSE lower than 0.0120, MAE lower than 0.007, and MAPE lower than 0.9%, which can more accurately predict SOH for lithium-ion batteries.

The further works can be considered as follows: (1) SOH and RUL prediction for lithium-ion batteries considering practical applications; (2) Application of the latest machine learning techniques in the prediction of SOH and RUL for lithium-ion battery, such as various variants and improvements of the transformer; (3) Ways and ideas to combine the physical–chemical laws of lithium batteries and artificial intelligence technologies.

Author Contributions: Conceptualization, methodology, software, validation, formal analysis, investigation, writing—original draft preparation, visualization, Y.T.; conceptualization, methodology, validation, investigation, writing—review and editing, supervision, project administration, funding acquisition, J.W.; methodology, validation, investigation, Y.Y.; conceptualization, formal analysis, Y.S.; supervision, project administration, funding acquisition, J.Z. All authors have read and agreed to the published version of the manuscript.

Funding: This work was supported by the National Natural Science Foundation of China under Grant 72071183, and the Research Project Supported by Shanxi Scholarship Council of China under Grant 2020-114.

Data Availability Statement: Not applicable.

Acknowledgments: In particular, thanks to the NASA Ames Center of Excellence Diagnostic Center for providing the experimental data.

Conflicts of Interest: The authors declare no conflict of interest.

References

- Rajaeifar, M.A.; Ghadimi, P.; Raugei, M.; Wu, Y.; Heidrich, O. Challenges and recent developments in supply and value chains of electric vehicle batteries: A sustainability perspective. *Resour. Conserv. Recycl.* **2022**, *180*, 106144. [[CrossRef](#)]
- Xiong, R.; Li, L.; Tian, J. Towards a smarter battery management system: A critical review on battery state of health monitoring methods. *J. Power Sources* **2018**, *405*, 18–29. [[CrossRef](#)]
- Shen, M.; Gao, Q. A review on battery management system from the modeling efforts to its multiapplication and integration. *Int. J. Energy Res.* **2019**, *43*, 5042–5075. [[CrossRef](#)]
- Shen, P.; Ouyang, M.; Lu, L.; Li, J.; Feng, X. The co-estimation of state of charge, state of health, and state of function for lithium-ion batteries in electric vehicles. *IEEE Trans. Veh. Technol.* **2017**, *67*, 92–103. [[CrossRef](#)]
- Lai, X.; Gao, W. A comparative study of global optimization methods for parameter identification of different equivalent circuit models for Li-ion batteries. *Electrochim. Acta* **2019**, *295*, 1057–1066. [[CrossRef](#)]

6. Wang, Y.; Gao, G.; Li, X.; Chen, Z. A fractional-order model-based state estimation approach for lithium-ion battery and ultra-capacitor hybrid power source system considering load trajectory. *J. Power Sources* **2020**, *449*, 227543. [[CrossRef](#)]
7. Cheng, G.; Wang, X.; He, Y. Remaining useful life and state of health prediction for lithium batteries based on empirical mode decomposition and a long and short memory neural network. *Energy* **2021**, *232*, 121022. [[CrossRef](#)]
8. Rechkemmer, S.; Zang, X. Empirical Li-ion aging model derived from single particle model. *J. Energy Storage* **2019**, *21*, 773–786. [[CrossRef](#)]
9. Li, K.; Wang, Y.; Chen, Z. A comparative study of battery state-of-health estimation based on empirical mode decomposition and neural network. *J. Energy Storage* **2022**, *54*, 105333. [[CrossRef](#)]
10. Geng, Z.; Wang, S.; Lacey, M.J.; Brandell, D.; Thiringer, T. Bridging physics-based and equivalent circuit models for lithium-ion batteries. *Electrochim. Acta* **2021**, *372*, 137829. [[CrossRef](#)]
11. Xu, N.; Xie, Y.; Liu, Q.; Yue, F.; Zhao, D. A Data-Driven Approach to State of Health Estimation and Prediction for a Lithium-Ion Battery Pack of Electric Buses Based on Real-World Data. *Sensors* **2022**, *22*, 5762. [[CrossRef](#)] [[PubMed](#)]
12. Ng, M.F.; Zhao, J.; Yan, Q.; Conduit, G.J.; Seh, Z.W. Predicting the state of charge and health of batteries using data-driven machine learning. *Nat. Mach. Intell.* **2020**, *2*, 161–170. [[CrossRef](#)]
13. Alipour, M.; Tavallaey, S. Improved Battery Cycle Life Prediction Using a Hybrid Data-Driven Model Incorporating Linear Support Vector Regression and Gaussian. *ChemPhysChem* **2022**, *23*, e202100829. [[CrossRef](#)] [[PubMed](#)]
14. Li, X.; Wang, Z. Prognostic health condition for lithium battery using the partial incremental capacity and Gaussian process regression. *J. Power Sources* **2019**, *421*, 56–67. [[CrossRef](#)]
15. Li, Y.; Abdel-Monem, M. A quick on-line state of health estimation method for Li-ion battery with incremental capacity curves processed by Gaussian filter. *J. Power Sources* **2018**, *373*, 40–53. [[CrossRef](#)]
16. Ströbel, M.; Pross-Brakhage, J.; Kopp, M.; Birke, K.P. Impedance Based Temperature Estimation of Lithium Ion Cells Using Artificial Neural Networks. *Batteries* **2021**, *7*, 85. [[CrossRef](#)]
17. Wu, B.; Han, S.; Shin, K.G.; Lu, W. Application of artificial neural networks in design of lithium-ion batteries. *J. Power Sources* **2018**, *395*, 128–136. [[CrossRef](#)]
18. Dai, H.; Zhao, G.; Lin, M.; Wu, J.; Zheng, G. A novel estimation method for the state of health of lithium-ion battery using prior knowledge-based neural network and Markov chain. *IEEE Trans. Ind. Electron.* **2019**, *66*, 7706–7716. [[CrossRef](#)]
19. Yang, Y.; Wen, J.; Shi, Y.; Zeng, J. State of Health Prediction of Lithium-Ion Batteries Based on the Discharge Voltage and Temperature. *Electronics* **2021**, *10*, 1497. [[CrossRef](#)]
20. Feng, X.; Weng, C.; He, X.; Han, X.; Lu, L.; Ren, D.; Ouyang, M. Online state-of-health estimation for li-ion battery using partial charging segment based on support vector machine. *IEEE Trans. Veh. Technol.* **2019**, *68*, 8583–8592. [[CrossRef](#)]
21. Jia, J.; Liang, J.; Shi, Y.; Wen, J.; Pang, X.; Zeng, J. SOH and RUL Prediction of Lithium-Ion Batteries Based on Gaussian Process Regression with Indirect Health Indicators. *Energies* **2020**, *13*, 375. [[CrossRef](#)]
22. Yang, D.; Zhang, X.; Pan, R.; Wang, Y.; Chen, Z. A novel Gaussian process regression model for state-of-health estimation of lithium-ion battery using charging curve. *J. Power Sources* **2018**, *384*, 387–395. [[CrossRef](#)]
23. Kheirkhah-Rad, E.; Moeini-Aghetaie, M. A novel data-driven SOH prediction model for lithium-ion batteries. In Proceedings of the 2021 31st Australasian Universities Power Engineering Conference (AUPEC), Perth, Australia, 26–30 September 2021; pp. 1–6. [[CrossRef](#)]
24. Tan, Y.; Zhao, G. Transfer Learning With Long Short-Term Memory Network for State-of-Health Prediction of Lithium-Ion Batteries. *IEEE Trans. Ind. Electron.* **2020**, *67*, 8723–8731. [[CrossRef](#)]
25. Khumprom, P.; Yodo, N. Data-driven Prognostic Model of Li-ion Battery with Deep Learning Algorithm. In Proceedings of the 2019 Annual Reliability and Maintainability Symposium (RAMS), Orlando, FL, USA, 28–31 January 2019; pp. 1–6. [[CrossRef](#)]
26. Chaoui, H.; Ibe-Ekeocha, C.C. State of Charge and State of Health Estimation for Lithium Batteries Using Recurrent Neural Networks. *IEEE Trans. Veh. Technol.* **2017**, *66*, 8773–8783. [[CrossRef](#)]
27. Chen, Z.; Song, X.; Xiao, R.; Shen, J.; Xia, X. State of Health Estimation for Lithium-Ion Battery Based on Long Short Term Memory Networks. In Proceedings of the 2018 Joint International Conference on Energy, Ecology and Environment (ICEEE) and International Conference on Electric and Intelligent Vehicles (ICEIV), Melbourne, Australia, 21–25 November 2018; pp. 1–6. [[CrossRef](#)]
28. Bezha, M.; Nanahara, T.; Nagaoka, N. Development of Fast SoH Estimation of Li-Ion Battery Pack/Modules Using Multi Series-Parallel based ANN Structure. In Proceedings of the 2021 IEEE 12th Energy Conversion Congress & Exposition-Asia (ECCE-Asia), Singapore, 24–27 May 2021; pp. 1719–1724. [[CrossRef](#)]
29. Qu, J.T.; Liu, F.; Ma, Y.X.; Fan, J.M. A Neural-Network-Based Method for RUL Prediction and SOH Monitoring of Lithium-Ion Battery. *IEEE Access* **2019**, *7*, 87178–87191. [[CrossRef](#)]
30. Cai, W.; Wang, Y.; Ma, J.; Jin, Q. CAN: Effective cross features by global attention mechanism and neural network for ad click prediction. *Tsinghua Sci. Technol.* **2022**, *27*, 186–195. [[CrossRef](#)]
31. He, M.; Xue, X.; Zhang., X.; Zhou., C. A Bike-sharing Demand Predicting Model with Integrating Temporal Convolutional Network and Self-Attention. In Proceedings of the International Conference on Electronic Information Engineering and Computer Science (EIECS), Changchun, China, 23–26 September 2021; pp. 278–281. [[CrossRef](#)]
32. Feng, A.; Zhang, X.; Song, X. Unrestricted Attention May Not Be All You Need—Masked Attention Mechanism Focuses Better on Relevant Parts in Aspect-Based Sentiment Analysis. *IEEE Access* **2022**, *10*, 8518–8528. [[CrossRef](#)]

33. Liu, D.; Liu, J.; Luo, Y.; He, Q.; Lei, D. MGATMDA: Predicting microbe-disease associations via multi-component graph attention network. In *IEEE/ACM Transactions on Computational Biology and Bioinformatics*; IEEE: Piscataway, NJ, USA, 2021; p. 29. [[CrossRef](#)]
34. Zhu, Y.; Zhao, C.; Guo, H.; Wang, J.; Zhao, X.; Lu, H. Attention CoupleNet: Fully Convolutional Attention Coupling Network for Object Detection. *IEEE Trans. Image Process.* **2018**, *28*, 113–126. [[CrossRef](#)]
35. Saha, B.; Goebel, K. Battery Data Set. Available online: <http://ti.arc.nasa.gov/tech/dash/pcoe/prognostic-data-repository/> (accessed on 18 February 2020).
36. El-Dalahmeh, M.; Al-Greer, M.; El-Dalahmeh, M.; Short, M. Time-Frequency Image Analysis and Transfer Learning for Capacity Prediction of Lithium-Ion Batteries. *Energies* **2020**, *13*, 5447. [[CrossRef](#)]